Electrical Engineering
https://doi.org/10.1007/s00202-025-03103-w

ORIGINAL PAPER

TSA-aided IT2FLC-(1+PD)-FOPID control for regulating the first-order plus time-delayed non-conventional multi-area power system with deregulation

Susmit Chakraborty[1] · **Arindam Mondal**[2]

Received: 4 October 2024 / Accepted: 26 March 2025

Abstract
Renewable energy appears to be a potential replacement for conventional sources of energy in terms of reliable power delivery. Large-scale electrical grids can have significant synchronization mismatches between components owing to delayed communication or systems. Engineers face many obstacles when seeking to replace traditional sources with non-conventional sources of energy since the production characteristics of renewable power plants constantly change due to climatic conditions. A time-delayed AGC or automatic generation control system can be handled using clever control, such as type-II-fuzzy-aided multi-layer control. This paper presents a unique control approach for a first-order plus time-delay (FOPTD) based on a multi-area power system (MAPS) with deregulation known as the FUZZY-(1+PD)-FOPID controller. They are trained using a variety of algorithms, including the fire-bug swarm optimization (FSO), Levenberg–Marquardt method of optimization (LMA), particle swarm technique for optimization (PSO), and tree-seed algorithm (TSA) while applying the integral-squared error (ISE) criteria to illustrate the efficacy of the controller settings. The MATLAB simulation platform sketches and simulates the complete system, including the controller. The acquired parameters, such as settling time (ST), overshoot (OS), and undershoot (US), are used to examine the simulation findings. The TSA-adjusted suggested controller outperforms TSA:PID and TSA:FOPID in OS, US, and ST specifications, with 88–100% better OS, 8–10% better US for frequency errors, and 38–98% better US for tie-bar power errors. The suggested combination of the controller and the optimization technique has also proven its efficacy as it outperforms other combinations and other optimization techniques in terms of OS, US, and ST for $Del\,P_i$, with a 44–98% better OS, 17–85% better US, and 35–62% better ST in the case of $Del\,P_{ties}$ between distinct regions.

Keywords Load frequency control (LFC) · Solar power plant · Wind power plant · Ocean-thermal power plant · Interval Type-II fuzzy control · First-order plus time delay (FOPTD) · Tree-seed algorithm (TSA)

List of symbols

ACE	Area control error
A	Aqua electrolyzer
AGC	Automatic generation control
BD	Boiler-dynamics
ΔF_i	Frequency error
$\Delta P_{tie_{ij}}$	Tie-line error
FC	Fuel cell
FO	Fractional order
FOPTD	First-order plus time delay
FPIDF	Fuzzy-based PID filter
FSO	Firebug swarm optimization
g^{ij}	Firing angle
GM	Gain margin
GRC	Governor rate constraint
HBA	Honey badger algorithm
IGSA	Improved gravitational search algorithm
ITSE	Integral of time-squared error
IT2FLC	Interval-type-II fuzzy logic controller
J	Loss Function
K_d	Differentiation constant of the controller
K_i	Integration constant of the controller

✉ Arindam Mondal
arininstru@gmail.com

[1] Department of Computer Science and Engineering (Cyber Security and Data Science), Brainware University, Barasat, West Bengal, India

[2] Present Address: Department of Electrical Engineering, Dr. B.C. Roy Engineering College, Durgapur, West Bengal 713206, India

Published online: 02 May 2025

K_p	Proportionality constant of the controller
$lambda$	Integration degree
LFC	Load frequency control
LMA	Levenberg–Marquardt algorithm
LN	Large-negative
LP	Large-positive
MAPS	Multi-area power system
MF	Membership function
MN	Medium-Negative
MP	Medium-Positive
mu	Differentiation degree
mu_F	Membership function
OS	Overshoot
PEM	Proton exchange membrane
PM	Phase margin
PS	Power system
RE	Renewable energy
RLP	Random load perturbation
SN	Small-Negative
SP	Small-Positive
ST	Settling time
τ	Time function of FOPTD
TSA	Tree-seed algorithm
UC	Ultra-capacitor
US	Undershoot
Z	Zero
$\zeta(p)$	MembershipVector

1 Introduction

1.1 Background

As a way to reduce voltage and frequency oscillations caused by variations in load and demand, load frequency control (LFC) [1] has grown in importance in correlated MAPS in recent decades [2]. A power system's (PS) normal operational state is defined by constant frequency and voltage profiles with a specific degree of system dependability [3]. Because demand is increasing, more control regions are connected, which leads to more system disturbances. This clearly leads to an imbalance between supply and demand. For more smooth PS network control, frequency mismatches in imbalanced scenarios must be reduced. LFC is essential for the decrease in frequency and tie-bar power error caused by changes in generation and demand. The complexity of the PS network is increasing with the inclusion of integrated renewable energy (RE) sources such as ocean-thermal, wind, and solar power plants [4].

1.2 Challenges and scope

Non-renewable fossil fuel stocks are steadily being depleted by the power system (PS) sector's growing reliance on renewable energy (RE) sources. Renewable energy sources have enormous promise and substantial environmental advantages. According to a research by Arya et al. in citearya2021cascade, the efficiency of energy transmission from these sources keeps improving as a result of continuous cost reductions in the renewable energy industry. However, because renewable energy technologies are inherently variable, integrating them presents challenges. According to a review by Hu et al., strong control and stability strategies must be utilized to prevent possible issues such as output power desynchronization and communication interruptions with the grid brought on by weather changes.[5]. The transmission and processing of data across remote communication channels often result in delays, varying from a few seconds to extended periods, depending on the communication infrastructure, as discussed in [6]. The forthcoming approach of implementing open communication channels, such as DGS aggregators, is anticipated to exacerbate delays during high data exchange periods, which could potentially affect the synchronization of power systems, as detailed by Abd et al. in [7]. It is important to recognize that communication delays affect the Automatic Generation Control (AGC) system's damping behavior, which may result in power system instability and synchronization problems. These difficulties highlight the need for creative fixes and cutting-edge technology to improve the dependability and effectiveness of integrating renewable energy sources into the infrastructure of the power industry.

1.3 Literature review and motivation

The literature offers a variety of regulating solutions and tuning techniques to deal with this problem and raise the frequency label and tie-line power efficiency levels in the PS. Chakraborty et al. implemented fuzzy-enabled 3DOF-PID controller [8] and type-II fuzzy controller [9] for a three-area AGC system consisting of an ocean-thermal power plant (OTPP). Babu et al. offered the PSO-assisted hybridized crow-search technique [10] to optimize the control with integral-minus tilt-derivative action using a filter. The gravitational search method may be used to tune a controller with dual PI action [11]. Over the last several years, academics have concentrated on developing the subject of fractional-order (FO) control, which A emphasizes the use of fractional calculus in the development of control systems. This section discusses the use of FO differentiation and integration operators in real-world process modeling, as well as useful control rule ideas. Fractional operators provide the bedrock for less parameterized and more accurate computational modeling

of processes from multiple fields including mechanical engineering [12] section, electrical [13], medicine [14], and some relaxation mechanisms [15]. However, due to their distinct properties, they are utilized to design controllers that are more robust to process fluctuations than typical integer-order controllers. Some of the most real-world instances of fixed-structure FO controllers including FO-PD, FO-PI, and FOPID controllers, were first implemented by Podlubny [16]. In order to stabilize and balance the frequency for the problem on LFC, Shouran et al. [17] applied the bees approach to the PID, fuzzy-based PID filter (FPIDF), and fractional-order PID (FOPID) controller. Hakimuddin et al. tuned the PID controller in a MAS using the BFA technique of optimization [18]. For PV system component identification, Arandian and his colleagues offer an efficient metaheuristic approach based on tunicate swarm optimization [19]. A sperm swarm-based optimization (MSSO) method was presented by Eslami et al. for the PS domain's ideal damping controller design. [20]. Adaptive rat swarm optimization (ARSO), a new study by Moghadam et al., is a successful optimization method for handling challenging optimization issues that are based on rat swarm behavior [21]. The modified FFO technique was proposed by Mohanty et al. [22] to enhance the linear quadratic controller's weighted matrices. The COKHA technique [23] was introduced by Goswami et al. to solve multi-source AGC problems. Elsisi and colleagues presented a novel supervisory fuzzy nonlinear sliding mode control technique [24]. In the AGC problem Fuzzy-PID controller with Hybrid alopex-based hybrid optimization has been developed by Nayak et al. [25]. In a deregulated setting, Biswas et al. tuned the AGC using the GOA [26]. Hashim et al. have recently created the honey badger algorithm (HBA) [27] to solve several optimization issues. Craziness factor entitled crow-search algorithm tuned optimally designed fuzzy PID controller recently used by Sahu et al. [28]. To investigate the LFC of a two-area connected PS, an improved gravitational search algorithm (IGSA)-aided fuzzy logic (Type-I) controller is considered [29]. A.K. Mohapatra and associates have developed a fuzzy controller and modeling of flexible AC transmission system devices for electric vehicle-injected AGC-PS in [30]. P. C. Sahu's analysis examines the impact of electric vehicles on RE-based microgrids, focusing on frequency profile improvement using an optimized FO-Fuzzy PSS approach [31]. Sahu et al. have also designed a robust Type-2 fuzzy cascade PIF controller with CSA tuning for resilient frequency stability of a PV and wind penetration complicated PS [32]. For LFC with communication latency, a fuzzy type-II controller is additionally used. [33]. The LFC problem of a FOPTD-based renewable three-area deregulated hybrid PS is addressed by utilizing FUZZY-3DOF-PID control [34]. Type-l fuzzy logic controllers are improved to type-II fuzzy logic controllers by assigning grades to the inherently fuzzy membership functions (MFs). Since the membership in type-II fuzzy is a function rather than a point value at each value of the variable, it may be seen as a three-dimensional set that offers an extra degree of flexibility for handling uncertainties [35]. In [36], a new QO-PFA directed FO cascaded fuzzy-II control system for LFC of thermo-electric generator-based hybrid PS has been investigated. Table 1 is a historical survey of the referred work. In this table, 'Y' represents the yes, which signifies that the corresponding item is present in the various references utilized here, and 'N' represents the no, which shows the lack of the specific item in the reference.

1.4 Contribution

This article aims to introduce two control layers, namely (1+PD) and FOPID units, to enhance the LFC action of the interval-type-II fuzzy logic controller (IT2FLC). Here, the authors have implemented a 3-layer controller for a three-area renewable-based hybrid interconnected deregulated PS network. This controller, called IT2FLC-(1+PD)-FOPID, takes into consideration variable FOPTD, some nonlinearities like dynamics in the boiler (BD) and constraints of the governor rate (GRC), and a few energy storage devices like fuel cell units and aqua electrolyzers. The tree-seed algorithm (TSA) is the recommended method for choosing the right controller parameter values in this chapter. Natural selection gave rise to TSA, a powerful population-based stochastic metaheuristic optimization technique. Based on the link between trees and seeds, TSA was created by Kiran [38] to address challenges with continual optimization. TSA uses a three-layer controller to adjust parameters like K_{p1}, K_{d1}, K_{p2}, K_{i2}, K_{d2} and other parameters like the exponential of the differentiator (μ) and integrator (λ) for a network of interconnected, deregulated hybrid PSs that consists of both conventional (thermal, nuclear, and hydro-electric) and renewable (wind, solar, and ocean thermal) energy sources. To increase the effectiveness of the suggested controller, additional optimization techniques like PSO [10], FSO [39], and LMA [40] are also used.

Based on the literature survey, the major earnings in the current working are enumerated below:

1. A linearized model of a non-conventional-based hybrid power system (PS) is developed using Linear Feedback Control analysis. This model investigates the impact of delay, specifically in the context of a first-order plus time-delay (FOPTD) system, on the system's operational performance. Hybrid power systems combine multiple energy sources to enhance reliability and efficiency, reducing dependency on fossil fuels. Understanding these dynamics is crucial for optimizing hybrid power systems' performance and implementing timely inter-

Table 1 The taxonomy of publications on LFC utilizing various systems and constraints

References	AGC systems		Area type	Algorithms	Controllers	A_E	F_C	U_C	GRC	Time-Delay
	conventional sources	Renewable sources								
[1]	Y	N	2	ICA	FTI$^{\lambda}$DN	N	N	N	N	N
[2]	Y	Y	2	CASO	PI	Y	Y	Y	Y	Y
[4]	Y	Y	2	PSO	Fuzzy-PID	N	N	N	N	N
[37]	Y	N	2	ICA	C − I$^{\lambda}$D$^{\mu}$N	N	N	N	N	N
[8]	Y	Y	3	FSO	FUZZY-3DOF-PID	N	N	N	N	N
[14]	Y	Y	3	WA	Fuzzy-FOPID	N	Y	N	N	N
[9]	Y	Y	2	LMA	type-II-Fuzzy-FOPID	N	N	N	N	N
[10]	Y	N	3	hCA-PSO	I-TDN	N	N	N	Y	N
[34]	Y	Y	3	TSA	Fuzzy-3DOF-PID	Y	Y	Y	Y	Y
This Work	Y	Y	3	TSA	IT2FLC-(1+PD)-FOPID	Y	Y	Y	Y	Y

ventions to enhance the operational effectiveness of these diverse energy sources.

2. This study explores the impact of nonlinearities and communication delays on frequency instability issues in power systems. It aims to understand the complex nature of frequency regulation challenges and offer practical recommendations for optimizing control strategies. The research aims to foster more robust and resilient power grid solutions amidst evolving technological demands and dynamic operating conditions.
3. The study supports the implementation of the Interval Type-2 Fuzzy Logic Controller combined with Proportional-Derivative action and Fractional Order Proportional-Integral-Derivative control (IT2FLC-(1+PD)-FOPID) as an effective control strategy for mitigating system-wide issues caused by varying oscillations and unpredictable time lags. This advanced control methodology can enhance system stability and performance, offering a promising opportunity for optimizing control mechanisms in complex operational environments.
4. Control systems use various optimization techniques, such as Particle Swarm Optimization (PSO) [10], Firebug Swarm Optimization (FSO) [39], Levenberg–Marquardt algorithm (LMA)[40], and tree-seed algorithm (TSA) [41]. These methods enhance controller performance, functionality, and responsiveness across various systems. By integrating these techniques, control systems can adapt to dynamic operational conditions and meet specific requirements. This commitment to precision and efficacy in control engineering leads to the creation of intelligent and adaptive control mechanisms.
5. The proposed scheme incorporates random load perturbation, enhancing its performance and efficacy in load frequency control (LFC) research. This innovative approach demonstrates adaptability and resilience in real-world power systems under varying conditions. The integration of RLP perturbation pushes the boundaries of traditional LFC methodologies. It represents a paradigm shift toward more dynamic, responsive, and efficient power system control and stability analysis approaches.

2 Methodology

This study attempts to consider a deregulated environment by taking into consideration non-traditional resources, including OTPP, solar, and wind. Each unit is projected to have 1400 MW as the total output power of the PS considered here. The first region's power system consists of 1000 MW of thermal units and 400 MW of solar power plants. The second and third regions, as seen in Fig. 1, include nuclear (1000 MW)-OTPP (500 MW) and wind (600 MW)-hydro (1000 MW) power

plants. To ensure the effectiveness of the suggested controller in an operational setting, several nonlinearities are added to the thermal unit and nuclear unit, as shown in Fig. 7(a-c). Dynamics of boilers (BD), constraints on governor rate (GRC), and first-order plus time-delay (FOPTD) are some of these nonlinearities. In this study, GRC was calculated to be 3% every minute. It is common practice to consider 0.05% nonlinearity for hydro-system and backslash nonlinearity of 2%. [42]. This study investigates delay-dependent stability in a deregulated environment. Here, a delay (FOPTD) produced by synchronization loss across several linked power plants is taken into consideration just before each controller and is stated by Eq. 3 [43]. Taking into account all of the aforementioned elements and PS units, the hybrid, multi-area deregulated PS is controlled by a multilayer intelligent type-2 fuzzy-based controller, which is helped by the TSA technique for tweaking controller settings. When the suggested control mechanism is in operation, the frequency and tie-line power errors are significantly minimized. The following portion of this article examines each area of the PS in further depth.

3 Proposed controller and PS constraints

The suggested controller (IT2FLC-(1+PD)-FOPID) in this publication consists of three layers. The ACE signal (area control error) along with its derivative signal (ACE-D) are the inputs of the interval type-II fuzzy unit (IT2FLC), which makes up the first portion. This unit's output is supplied into the (1+PD) later level of control, and the output of that stage is then fed back into the last FOPID block. Because the three governing units are cascaded, disruptions tend to be swiftly eliminated by the system before spreading to other parts of it. The many controller units and various limitations taken into consideration are described in the next subsections.

3.1 FOPID controller

FOPID refers to Fractional Order P-I-D. Podlubny implemented it in [44]. The FOPID controller performs better than the PID owing to its wider range of freedom degree and better resilience [45]. However, the controller settings are more challenging to modify than those of the ordinary PID controller. Different design approaches have been proposed for FOPID [46] and [47]. Aside from the three parameters (K_p, K_d, $and K_i$), there are two additional settings (λ and μ) to consider when representing a FOPID controller. Equation 1 describes the transfer function of a FOPID controller. Figure 2 shows the anatomical representation of the FOPID controller.

$$G_{FOPID}(s) = \frac{Y_F(s)}{E_F(s)} = K_{p2} + s^{\mu} K_{d2} + \frac{K_{i2}}{s^{\lambda}} \tag{1}$$

where μ = derivative-degree, λ = integration-degree.

The fractional order of the FOPID controller makes it more robust to variations and uncertainties within the power system parameters, which is crucial for LFC since load and power generation can fluctuate unpredictably.

3.2 (1+PD) unit

Two parameters, such as $K_{P1}\&K_{D1}$, are in charge of controlling the output signal of the IT2FLC unit (F) in the second layer of the proposed controller. Figure 3 shows the unit's graphical representation, and Eq. 2 may be used to build the transfer function of (1+PD).

$$\mathrm{G_{(1+PD)s}} = 1 + \mathrm{K_{P1}} + \mathrm{sK_{D1}} \tag{2}$$

The 1+PD term adds a proportional-derivative action to the controller, which is instrumental in reducing the rise time and settling time, leading to faster corrections in frequency deviations as well as tie-line error deviations.

3.3 IT2FLC unit

The fuzzy technique (FLC) is a multi-valued sensible approach that works well for dealing with erroneous, fine-grained data in a batch. An FLC consists of multiple rules. The lack of information about how to create these guidelines is something that occurs rather regularly. Fuzzy logic controllers (FLCs) can effectively manage uncertain circumstances [50] [51]. Zadeh developed both type-I and type-II FLCs for control [52]. Fuzzy regulation can be used to deal with uncertainty and imprecision. It operates by analyzing statistical data about system activities. Any intermediate input state may be properly controlled using FLCs. The FLC approach has proven useful for control systems [53]. Type-I fuzzy controllers use ordinary fuzzy sets (OFS) to regulate interference systems. On the other hand, a type-II FLC has a hazy membership grade. As a result, memberships in fuzzy type-I sets (FS) are Crisp type [54], whereas Type-II FLC is known as Fuzzy-Fuzzy sets. Type-II FLCs also have main and secondary membership functions (PMF and SMF). SMF is simply the likelihood of PMF occurring, whereas PMF is a subset of [0,1] that results in a type-II MF grade. A type-II FS, designated by W and theoretically expressed by Eq. 3, has been emphasized by a type-II MF (2-MF), characterized as μ_{F}.

$$\mathrm{W} = \{((a,u), \mu_{\mathrm{F}}(a,u)) \mid \forall a \in X, \forall u \in G_a \subseteq [0,1]\} \\ \text{, in which } 0 \leq \mu_{\mathrm{F}}(\mathrm{a},\mathrm{u}) \leq 1 \tag{3}$$

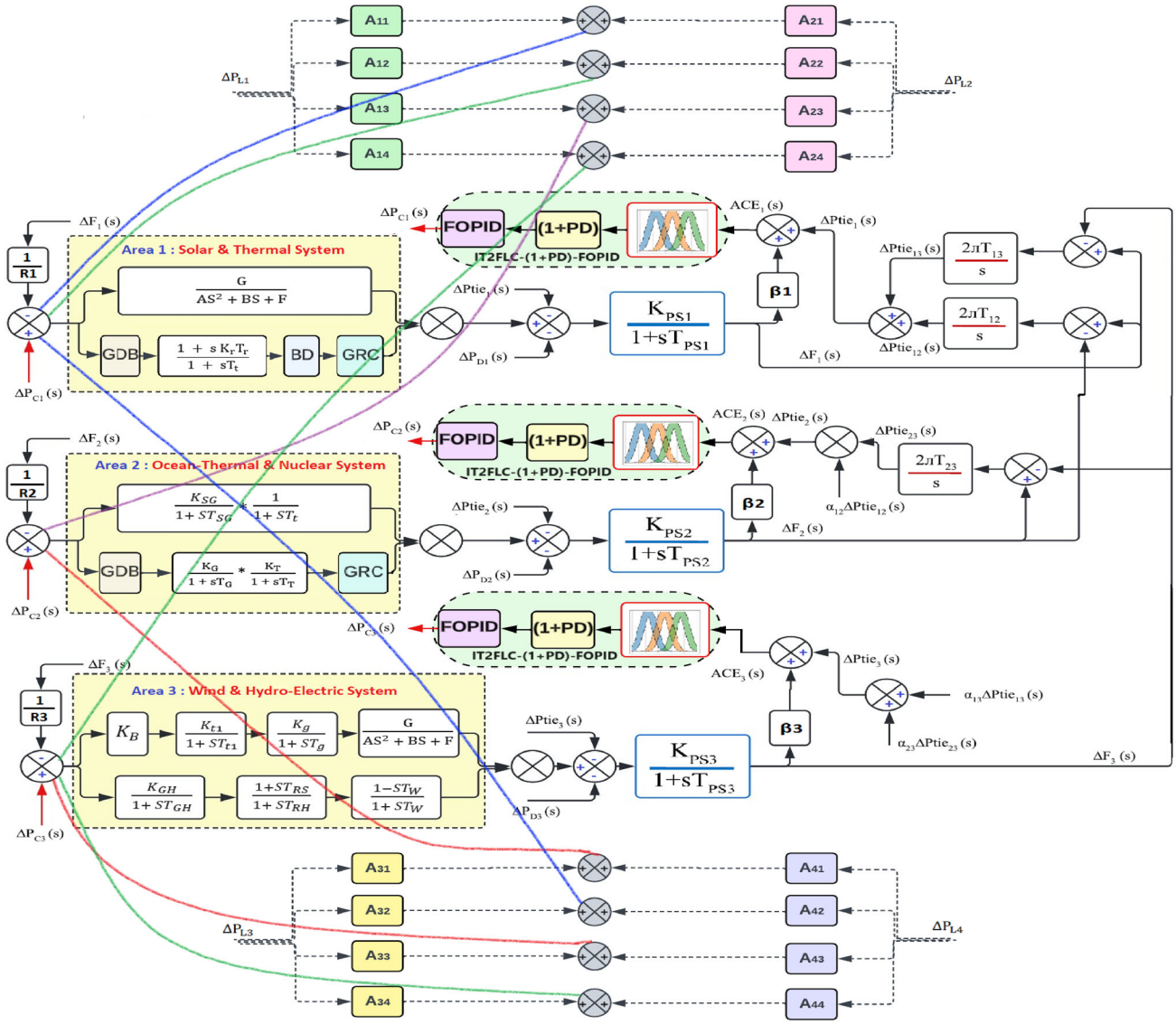

Fig. 1 Schematic illustration of the PS under consideration [34]

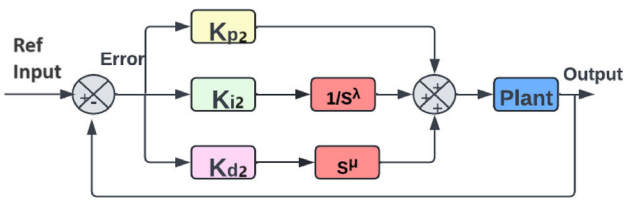

Fig. 2 Block Diagram of FOPID Controller [48]

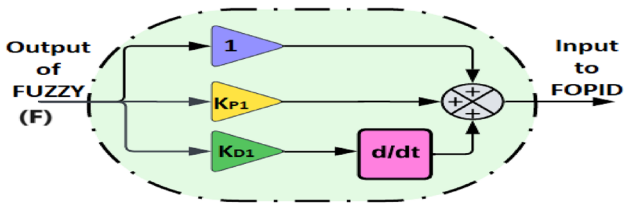

Fig. 3 Block Diagram of (1+PD) unit [49]

In this situation, the equation above can be written as Eq. 4

$$W = \int_{a\in X}\int_{u\in G_a} \frac{\mu_F(a,u)}{(a,u)}, G_a \subseteq [0,1] \tag{4}$$

where G_a is the initial MF a and μ_F is the 2-MF. The following are the general IT2FLC recommendations derived from the rules: The MF is G^{ij}, $(i, j = 1, 2, \ldots, N)$ where F_2^i, F_1^i are the first and second rules of 2-MF respectively, and a_1 and a_2 represent the inputs and G^{ij} consequent parameter, respectively. R : IF a_1 is F_1^i and a_2 is F_2^j. The firing set of R for singleton fuzzification is provided by (5) and (6).

$$F^{ij}(a) = \mu_{F_1^i}(a_1) \star \mu_{F_2^i}(a_2) \tag{5}$$

where ' $\star$ ' is t-norm operator.

$$F^{ij}(a) = \left[\underline{\mu}_{F_1^i} \star \underline{\mu}_{F_2^j}, \bar{\mu}_{F_1^i} \star \bar{\mu}_{F_2^j}\right] \equiv \left[\underline{g}^{ij}, \bar{g}^{ij}\right] \tag{6}$$

where the lower and higher firing levels of the m^{th} criteria are denoted by $\underline{g}^{ij}$, $\bar{g}^{ij}$, and the respective Mfs of $F^i(a)$ are denoted by $\underline{\mu}_{F_2^j}$, $\bar{\mu}_{F_1^i}$, respectively. As a result, (7) illustrates the output W.

$$\mu_F = \left[\underline{\mu}_F, \bar{\mu}_F\right] = \left[\underline{g}^{ij} \star \mu_{F^{ij}}, \bar{g}^{ij} \star \mu_{F^{ij}}\right] \tag{7}$$

The upper and the lower MFs are shown by (8).

$$\begin{aligned} \bar{\mu}_F &= \coprod_{m=1}^{l} \left(g^{-k} \star \mu_{G^m}\right) \\ &= \coprod_{m=1}^{l} \left(\bar{\mu}_{F_1^i(a_1)} \star \bar{\mu}_{F_2^i(a_2)} \star \mu_{G^l}\right) \\ \underline{\mu}_F &= \coprod_{m=1}^{l} \left(g^{-k} \star \mu_{G^m}\right) = \coprod_{m=1}^{l} \left(\underline{\mu}_F^i(a_1)^{\star} \underline{\mu}_{F_2^i(a_2)} \star \mu_{G^l}\right) \end{aligned} \tag{8}$$

The IT2FLC settings in this study are trained on the EKF as a basis. The Kalman filter (KF), which uses a recurrent technique and is updated based on prior estimates, reduces the need to keep past data for computations. Furthermore, the error amplification method is unsuitable for determining FLC control settings since it performs poorly in complicated process modeling, has a slow convergence time, and is subject to noise in input and output data. The EKF, on the other hand, is more commonly used because of its relationship to measurement and process noise. Considering the finite systems presented in (9) [55].

$$\begin{aligned} \zeta_{N_\zeta \times 1}(p+1) &= \zeta_{N_\zeta \times 1}(p) + n_{N_\zeta \times 1}(p) \\ y_{m_2 \times 1}(p) &= h[\zeta(p), x(p)] + v_{n_2 \times 1}(p) \end{aligned} \tag{9}$$

$\zeta(p)$ represents a vector of MF weights that includes process noise. $v(p)$ denotes the measured noise, and $h[\zeta(p), x(p)]$ denotes a function of activation for characterizing the nonlinear element of the system, and $y(p)$ is used as a model of measurement to generate a nonlinear IT2FLC. The IT2FLC is trained by EKF as follows:

Step I: Adjust the settings and standardize the data input and output to the IT2FLC block.

Step II: Compute the MF output vector in k^{th} step $y(p)$ based on (9).

Step III: Establish the derivative matrix for the weights using (10).

$$J(p) = \left[\frac{\partial y(p)}{\partial \zeta_1(p)}, \frac{\partial y(p)}{\partial \zeta_2(p)}, \ldots, \frac{\partial y(p)}{\partial \zeta_{N\zeta}(p)}\right] \tag{10}$$

Step IV: Calculate the estimation error vector as depicted in (11).

$$e(p) = y(p) - y(p) \tag{11}$$

Step V: Calculate the EKF gain with the formula depicted in (12).

$$K(p) = P(p)J(p)S(p) \tag{12}$$

Step VI: Update ζ, P and S as the formula prescribed in (13)

$$\begin{aligned} S(p) &= \left[R_n(p) + J^T(p)P(p)J(p)\right]^{-1} \\ \zeta(k+1) &= \zeta(p) + K(p) \cdot e(p) \\ P(k+1) &= P(p) - K(p)J^T(p)P(p) + Q_n(p) \end{aligned} \tag{13}$$

where y(p) is the optimal output and is regarded as the IT2FLC output. K(p) is the Kalman matrix, e(p) is the estimate error, and so on. Additionally, the error covariance matrix, the Jacobian IT2FLC output matrix in terms of weights, and the normalization matrix are designated as P(p), H(p), and A(p), respectively.

Figure 4 depicts a type-II FLC triangular type set. Figure 4a depicts the PMF, whereas Figs. 4b and 4c show the corresponding triangle and interval type membership functions. The darkened region in Fig. 4a represents two critical components: uncertainty and a description of all secondary grades in a type-II FLC-MF. Figure 5 depicts the complete block diagram of the IT2FLC, with all its components.

IT2FLC includes a type-II fuzzifier that converts all real-world integers to crisp values, a rule foundation for fuzzifying actions, a type reducer, and a defuzzifier. Real-world variables, such as Area Control Error (ACE) and its derivatives, are fed into the fuzzifier first. The rule foundation of a type-II FS facilitates the generation and processing of FSs. The type-reducer that calculates the centroid handles outputs encoded in type-II FSs. Type-reduced sets can be represented as $L_T R = [L_1, L_r]$, where L_1 and L_r are the two ends of type-reduced FSs. In the last phase, the type-I FSs are de-fuzzified to yield crisp edge outputs [56]. This fuzzy controller for LFC uses the subsequent rule base: If $ACE = F_{1i}$ and $\Delta ACE = F_{2i}$ then $u = C_i$ where F_{1i} and F_{2i} are interval type-II FSs, C_i = singleton matrix, and i = 1,2,....

Figure 6 illustrates the fuzzification of two inputs, area control error (ACE) and its derivatives (ΔACE), using positive and negative intervals type-II fuzzy. PMF of positive

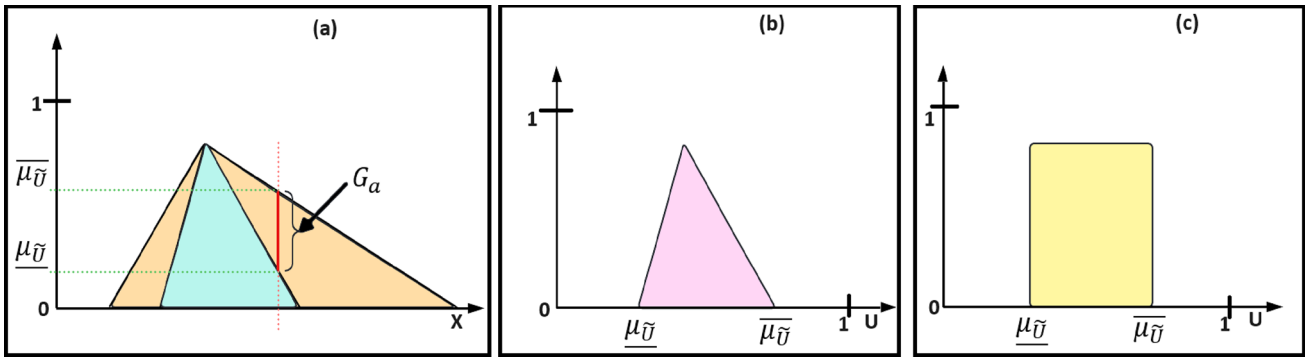

Fig. 4 A representation of the membership functions for (a) IT2FC and (b) triangle types (c) The membership function of interval type [8]

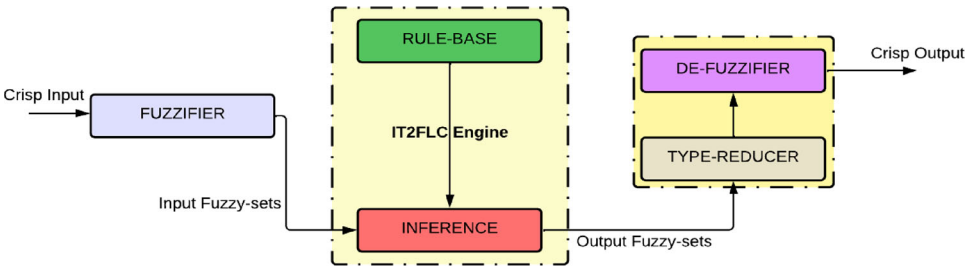

Fig. 5 IT2FLC block diagram [8]

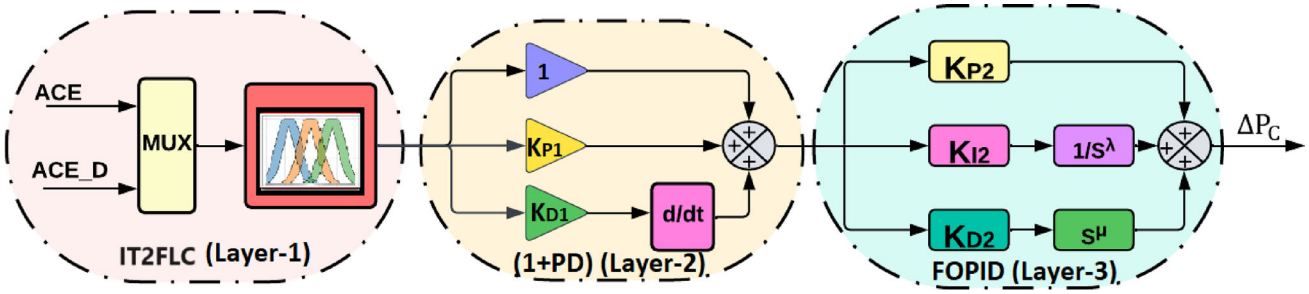

Fig. 6 IT2FLC-(1+PD)-FOPID controller schematic diagram

ACE, negative ACE, positive derivative of ACE, and negative derivative of ACE are represented by the notations: $\mu_p[\text{ACE}]$, $\mu_n[\text{ACE}]$, $\mu_p[\Delta\text{ACE}]$, $\mu_n[\Delta\text{ACE}]$. For a type-II fuzzy controller, the SMF remains constant. Equation 14 represents the mathematical representation of a type-I FS employed in the final de-fuzzification process.

$$\mu_p[\Delta\text{ACE}] = \begin{cases} 0 & (-\infty, -L_1) \\ \frac{(L_1+\Delta\text{ACE})}{2\,L_1} & (-L_1,\ L_1) \\ 1 & (\ L_1, \infty) \end{cases} \tag{14}$$

Table 2 summarizes the related rule base of the FLC unit, where LN, MN, SN, Z, SP, MP, and LP denote the MFs of the fuzzy operation: large-negative, medium-negative, small-negative, zero, small-positive, medium-positive, and large-positive, respectively.

In this paper, authors have implemented all three units as a cascaded 3-layer intelligent controller (IT2FLC-(1+PD)-FOPID) whose pictorial representation and complete transfer function are illustrated in Fig. 6 and Eq. 15.

Table 2 Parameter settings of the controllers using different algorithms [34]

		$\triangle ACE$						
		LN	MN	SN	Z	SP	MP	LP
ACE	LN	LP	LP	MP	MP	SP	$\bar{Z}$	SN
	MN	LP	MP	MP	SP	Z	Z	SN
	SN	LP	MP	SP	SP	Z	SN	MN
	Z	MP	SP	SP	Z	SN	MN	LN
	SP	MP	SP	Z	Z	SN	MN	LN
	MP	SP	Z	SN	SN	MN	MN	LN
	LP	SP	Z	SN	MN	MN	LN	LN

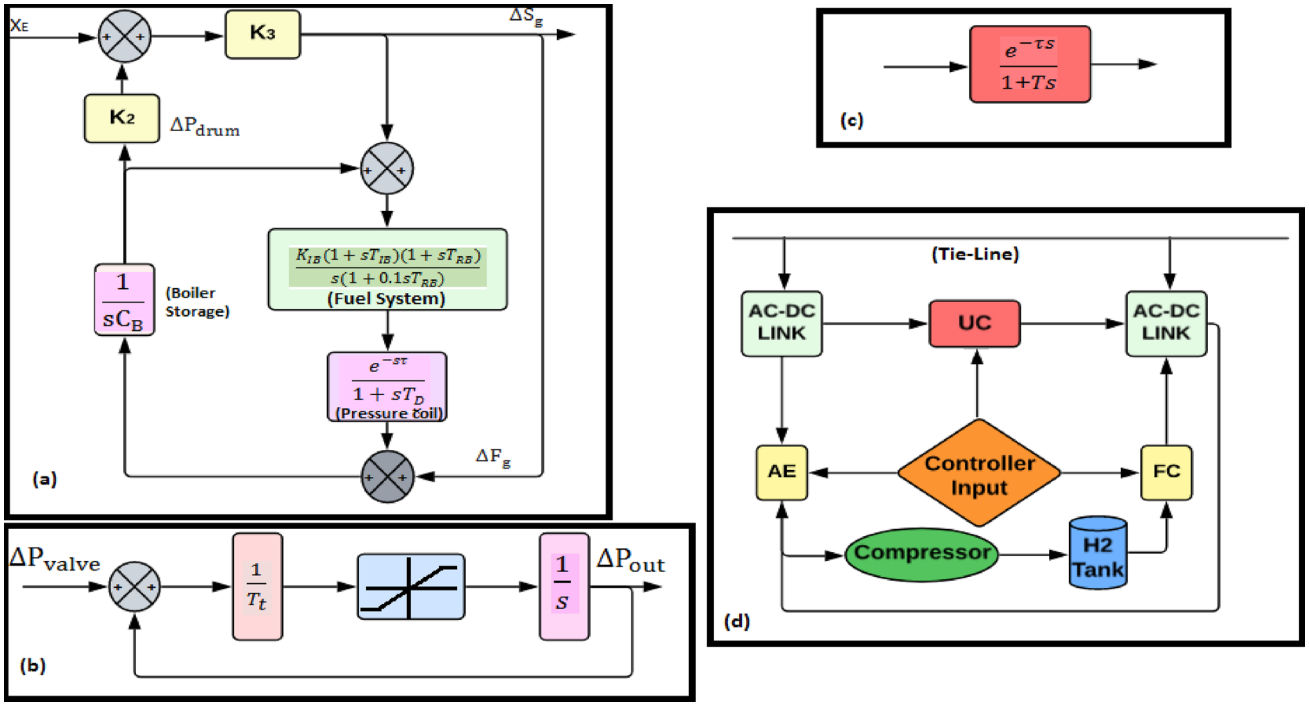

Fig. 7 Block diagram of the different constraints of PS: (a) Boiler Dynamics (b) Governor rate constraint (c) FOPTD (d) FC-AE-UC system [34]

$$
\begin{aligned}
\mathrm{G_C}(s) &= F * (1 + \mathrm{K_{P1}} + \mathrm{sK_{D1}}) * \left(\mathrm{K_{p2}} + \mathrm{s}^{\mu}\mathrm{K_{d2}} + \frac{\mathrm{K_{i2}}}{\mathrm{s}^{\lambda}} \right) \\
\mathrm{G_C}(s) &= F^{*}\Big[\mathrm{s}^{(\mu+1)}\mathrm{K_{D1}}\ \mathrm{K_{d2}} + \mathrm{s}^{\mu}\ (\mathrm{K_{d2}} + \mathrm{K_{d2}}\ \mathrm{K_{P1}}) \\
&+ \mathrm{sK_{D1}}\ \mathrm{K_{p2}} + \frac{\mathrm{K_{D1}}\ \mathrm{K_{i2}}}{\mathrm{s}^{(\lambda-1)}} + \frac{(\mathrm{K_{i2}}\ \mathrm{K_{P1}} + \mathrm{K_{i2}})}{\mathrm{s}^{\lambda}} \\
&+ \left(\mathrm{K_{p2}} + \mathrm{K_{P1}}\ \mathrm{K_{p2}}\right)\Big]
\end{aligned} \tag{15}
$$

3.4 First-order plus time delay (FOPTD)

Figure 7(c) illustrates a traditional closed-loop PS with negative-unity feedback. The first-order term in power systems represents primary dynamics, while time delay accounts for inherent system delays like sensor lag, communication delays, and generator response time. These delays are influenced by governor response delay, communication delays, load dynamics, and voltage regulation system response. This study characterizes latency of communication as a FOPDT with the following model:

$$D(S) = \frac{e^{-}\tau s}{(1 + Ts)} \tag{16}$$

3.5 Aqua electrolyzer (A_E) with fuel cell (F_C)

Aqua electrolyzer is frequently used as an extra source of energy to assist meet over a long-period power supply requirements. The main method used by A_E to produce variable power is electrolysis combined with strong hydrogen compression. Within a fuel cell (F_C), a proton exchange membrane (PEM) consumes the hydrogen that has been stored to provide energy that powers the load directly.

The characteristic function of the A_E is depicted in (17).

$$\mathrm{G_{AE}}(s) = \frac{K_{AE}}{1 + sT_{AE}} \tag{17}$$

Equation(18) represents the characteristic function of the FC.

$$\mathrm{G_{FC}}(s) = \frac{K_{FC}}{1 + sT_{FC}} \tag{18}$$

3.6 Ultra-capacitor(UC)

An ultra-capacitor (UC), also known as an electro-mechanical double-layer ultra-capacitor, may supply power to a deregulated system by balancing the generating and client demand. UC is utilized to calm down the sudden fluctuation and fulfill the specific load requirement. Compared to an FC, the energy density of a UC is substantially higher. The UC's stored-power calculations are as follows:

$$\mathrm{V_{UC}} = 0.5C(V_{in}^2 - V_{fi}^2) \tag{19}$$

V_{in} and V_{fi} are the beginning and final voltage levels of the UC, respectively, and C represents the capacitor in

farad units. The transfer function of UC is represented in the equation.

$$G_{UC}(s) = \frac{K_{UC}}{1 + sT_{UC}} \tag{20}$$

Figure 7(d) depicts the A_E, F_C, and U_C systems' block diagrams.

4 Mathematic assessment of the recommended design

In order to test the suggested hybrid power system's delay-based system stability, the study's authors introduce a random delay that can last anywhere from a few microseconds to hundreds of milliseconds. The system's dynamic outcomes can be improved significantly by selecting a different objective function.

4.1 Objective function analysis

According to optimal control theory, a closed-loop system's cost function is often seen as achieving the intended control target in the frequency or time domain. This cost function must be minimized by carefully adjusting the controller's free settings. One of the performance criteria for the optimization assignment in this study is the integral-time-squared error (ITSE). ITSE is represented by the letter J and is described as follows:

$$J = \int_0^{t_{\min}} t * ((\Delta f_1)^2 + (\Delta f_2)^2 + (\Delta f_3)^2 + (\Delta P_{tie1-2})^2 + (\Delta P_{tie1-3})^2 . dt) \tag{21}$$

where $t_{\min}$ is the minimal time of simulation for the optimizations; Δf_i and $\Delta P_{tie_{i-j}}$ are the frequency fluctuation of the ith area and small modifications in electrical power between the i^{th} and the j^{th} area, respectively. Analytical computation of ITSE requires the total error, represented by e(t) and written as follows:

$$e(t) = \sqrt{(\Delta f_1)^2 + (\Delta f_2)^2 + (\Delta f_3)^2 + (\Delta P_{tie1-2})^2 + (\Delta P_{tie1-3})^2}. \tag{22}$$

where e(t) is the unit step reference input closed-loop system error. There are no approximation methods used in the analytical procedure used to evaluate the ITSE cost function. Here is how we define E(s):

$$E(s) = \frac{\widetilde{B}(s) + \widetilde{D}(s)}{\widetilde{A}(s) + \widetilde{C}(s)} \tag{23}$$

The four variables A, B, C, and D all belong to viable integers of the polynomial. The closed-loop system is considered to be stable, and the integral of Eq. 23 exists. It is critical to note that for the system to be stable, the poles of E(s) must be located in the open left half of the s-plane. Using Parseval's theorem, the following integral is obtained:

$$J = \frac{1}{2\pi j} \int_{-j\infty}^{+j\infty} E(s) * E(-s)\ ds \tag{24}$$

Contour integration may be used to compute ITSE while evaluating just a finite number of related poles by substituting E(s) in Eq. 24 [57]. The integral J is calculated as follows, assuming that all the integrals surrounding the semi-circles at infinity are zero:

$$J = \sum_{res_{s_k}} \left(\frac{\widetilde{M}(s)}{\left(\widetilde{A}(s)\widetilde{A}(-s) - \widetilde{C}(s)\widetilde{C}(-s)\right)^3} * \frac{\widetilde{B}(-s)}{\widetilde{A}(-s) + \widetilde{C}(-s)e^{\tau s}} \right) \tag{25}$$

where

$M_{21}(s) = M'_{11}(s)\widetilde{A}(s) - 2M_{11}(s)\widetilde{A}'(s)$,

$M_{22}(s) = M'_{11}(s)\widetilde{C}(s) - (M'_{12}(s) - \tau M_{12}(s))\widetilde{A}'(s) - 2M_{12}(s)\widetilde{A}'(s) - 2M_{11}(s)(\widetilde{C}'(s) - \tau\widetilde{C}(s))$,

$M_{23}(s) = (M'_{12}(s) - \tau M_{12}(s))\widetilde{C}'(s) - 2M_{12}(s)(\widetilde{C}'(s) - \tau\widetilde{C}(s))$,

$M_{11}(s) = \widetilde{B}'(s)\widetilde{A}(s) - \widetilde{A}'(s)\widetilde{B}(s)$,

$M_{12}(s) = \widetilde{B}'(s)\widetilde{C}(s) - \widetilde{C}'(s)\widetilde{B}(s) + \tau\widetilde{B}(s)\widetilde{C}(s)$

where the following equation's roots yield the total number of residues, and the superscript $(\prime)$ denotes the derivative concerning s.

$$\left(\widetilde{A}(s)\widetilde{A}(-s) - \widetilde{C}(s)\widetilde{C}(-s)\right)^3 \tag{26}$$

Equation 26 can be expressed as:

$$(as^8 + bs^6 + cs^4 + ds^2 + e)^3 = 0 \tag{27}$$

The residue theory [58] is the foundation for the formula that follows, which is used to evaluate the residue of the i^{th} root of Eq. 27:

$$J_i = \lim_{s \to s_i} \frac{1}{2} \frac{\partial^2 \left(\left(\frac{\widetilde{M}(s)}{\widetilde{E}_i^3(s)} \right) * \left(\frac{\widetilde{B}(-s)}{\widetilde{A}(-s) + \widetilde{C}(-s)e^{\tau s}} \right) \right)}{\partial s^2} \tag{28}$$

$\widetilde{E}_i(s_i)$ represents the factorized version of the polynomial in Eq. 27. Using the sum of J_i's for each root of Eq. 25 and

Table 3 Maximum and minimum values for the proposed controller parameters using TSA approach

Controller parameters	K_{P1i}	K_{D1i}	K_{P2i}	K_{I2i}	K_{D2i}	λ	μ
mx	99.99	99.99	99.99	99.99	99.99	0.99	0.99
mn	0.01	0.01	0.01	0.01	0.01	0.01	0.01

considering the process variables (K, τ, T), authors establish a mathematical connection to assess the integral in Eq. 24 in terms of free controller settings. To calculate the precise value of the ITSE performance index, the controller coefficients for each root of the polynomial in Eq. 27 are fed into the function of Eq. 26.

4.2 System constraints

The anticipated AGC system has the following restrictions, which are expressed as a constrained optimization problem:

$$\begin{aligned} &K_{P1}^{mn} \le K_{P1i} \le K_{P1}^{mx} \\ &K_{D1}^{mn} \le K_{D1i} \le K_{D1}^{mx} \\ &K_{p2}^{mn} \le K_{P2i} \le K_{p2}^{mx} \\ &K_{d2}^{mn} \le K_{D2i} \le K_{d2}^{mx} \} \\ &K_{i2}^{mn} \le K_{I2i} \le K_{i2}^{mx} \\ &\lambda^{mn} \le \lambda_i \le \lambda^{mx} \\ &\mu^{mn} \le \mu_i \le \mu^{mx} \end{aligned} \tag{29}$$

The mn and mx symbols represent the lowest and greatest values of the controller parameters, respectively, prescribed in table 3. To optimize the above-specified parameters, this study uses the fire-bug swarm optimization (FSO), Levenberg–Marquardt algorithm (LMA), particle-swarm optimization (PSO), and tree-seed algorithm (TSA). The gain values of various storage devices such as AE, FC & UC are evaluated within a range from 0 to 1.

5 TS algorithm

The TS algorithm, or TSA, is a population-specific, random metaheuristic methodology of optimization technique that works well and occurs spontaneously. TSA, which is based on the association between seeds and trees, was developed by Kiran [38] to solve the issues with progressing optimization. The seeds carry out the mechanics of reproduction and propagation within the population of trees. Seeds are carried differently based on their architecture and morphologies. Some seeds adhere to fabrics, pelts, and feathers of birds. They are transferred from the tree to various locations. In this sense, when the seeds sprout under the proper circumstances, they grow into trees. For optimization issues, the ground is considered the search space in TSA. Trees and seeds both point to remedies for optimization issues. The exploitation and exploration procedures are critical to the remarkable efficacy of the meta-heuristic algorithms and the generation of a better-performing solution. Trees are dispersed at random over the search space during the exploration phase, and seeds with attributes comparable to the trees are used during the exploitation phase. The seeds are created using Eqs. 30 and 31.

$$M_{i,j} = R_{i,j} + a_{i,j} \times \left(D_j - R_{r,j}\right) \tag{30}$$

$$M_{i,j} = R_{i,j} + a_{i,j} \times \left(R_{i,j} - R_{r,j}\right) \tag{31}$$

The j^{th} dimensional parameter of the i^{th} tree is denoted by $R_{i,j}$; the j^{th} dimensional parameter of the r^{th} tree that is randomly generated in $[-1, 1]$ is denoted by $R_{r,j}$; the j^{th} dimensional parameter of the best location of the tree identified so far is denoted by D_j; and so on. The k^{th} seed produced from the i^{th} tree has these j^{th} dimensional characteristics. A haphazard selection is made from each seed during the search to find the best tree. The most crucial aspect is determining which equation will generate a new seed location. This selection is determined by the method's control parameter, search tendency (ST), which varies from 0 to 1. A higher ST number leads to faster convergence and stronger local search, whereas a lower ST value results in slower convergence but more powerful global search. Simply speaking, the ST component defines the TSA's exploration and exploitation capabilities. To begin a TSA search, Eq. (32) is used to generate launching tree sites that might solve the optimization problem.

$$R_{i,j} = LB_{j,\min} + r_{i,j}\left(HB_{j,\max} - LB_{j,\min}\right) \tag{32}$$

The search space's lower limit is $LB_{j,\min}$, the maximum limit is $HB_{j,\max}$, and r_{ij} is a number that is randomly produced for each dimension and location within the range of [0, 1]. To minimize, the most optimal answer from the population is chosen using Eq. (33).

$$D = \min\left\{f\left(\vec{R}_i\right)\right\} i = 1, 2, \ldots, N \tag{33}$$

The TSA has progressed till the termination criteria are satisfied. In this case, Fig. 8 displays the TSA basic flow diagram. To effectively attenuate the frequency and tie-line harmonics of power, the ideal control settings must be determined using a suitable target function (J). Furthermore, the system's productivity is determined by choosing the right J. J is considered ITSE in this case, as indicated by Eq. 21

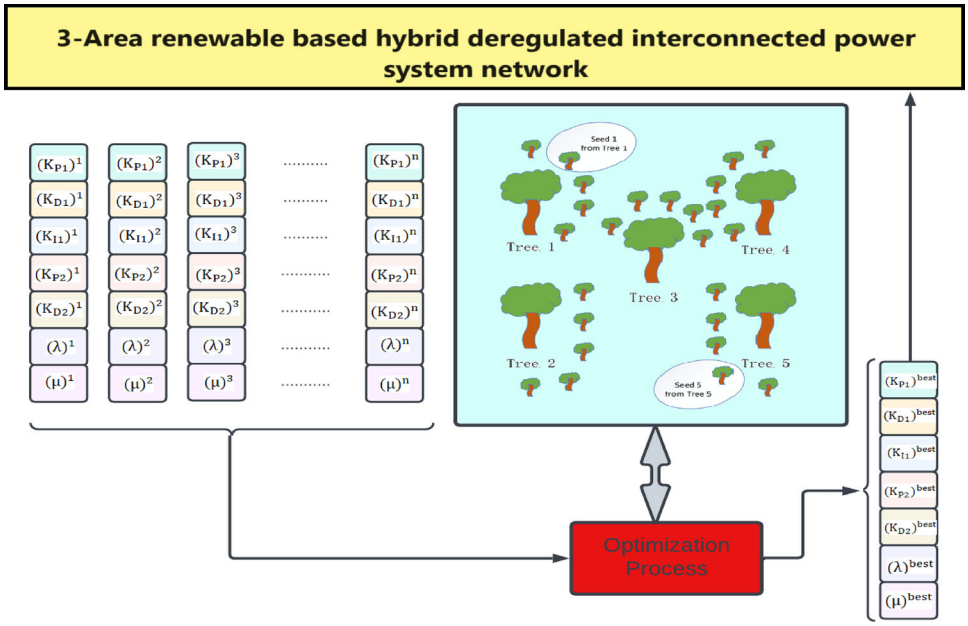

Fig. 8 TSA optimization Schematic [59]

and necessary for the system's optimal operation. Algo 1 highlights the TSA's extensive algorithmic foundation. The following relations are considered for the entire tuning process:

- $N = 1000$
- $S_{max} = 25\% of\, N = 250$
- $S_{min} = 10\% of\, N = 100$
- ST is observed using eq. 32
- Highest number of function findings = D * 10000
- D = Random between [0,1]

TSA method of optimization can be better understood by observing the flow process of the algorithm as given in fig. 9.

6 Simulation results

To simulate the three-area inter-connected, de-regulated hybridized PS, authors utilized a 2.80 GHz Intel Core-i7 CPU with 16 GB RAM and MATLAB/SIMULINK version 2020A. The parameters of the MATLAB simulation are viewed as variable step ODE45 solvers. The duration of simulation for each round of simulation has been configured at 70 s. The recommended algorithms TSA, LMA, FSO, and PSO are written in the.m file. To fine-tune the controller settings ($K_{P1i}, K_{D1i}, K_{P2i}, K_{d2i}, K_{i2i}, \lambda_i, \mu_i$), the maximum number of iterations is 200 in all cases. Starting with the system mentioned above and accounting for no communication delay, the research looks into the controllers TSA:PID, TSA:FOPID, TSA:IT2FLC-FOPID, and TSA:IT2FLC-(1+PD)-FOPID. As a result, the PS is subject to varying delays in communication, that can last anywhere from one to ten seconds. The identical system is subjected to simulations using all four previously described control strategies. The authors then used various highly efficient algorithms, including LMA, FSO, and PSO, to simulate the suggested controller to assess the effectiveness of TSA opti-

Algorithm 1 TSA framework

1: Step 1: Beginning the algorithmic process
2: Configure the size of the population(N).
3: Set the ST of the optimization workflow.
4: Set the dimensions of the concern (D).
5: Establish its termination instance.
6: Eq.32 generates a random tree position on the dimensional search space.
7: Employ the problem's objective function to evaluate the tree's position.
8: Choose the best answer (B) from Eq.33.
9: Step 2: Searching using Seeds
10: **for** all trees **do**
11: Decide the amount of seeds generated for this tree.
12: **for** all seeds **do**
13: **for** all D **do**
14: **if** rand is less than ST **then** Adjust this dimension with Eq.30.
15: **else**Adjust D using Eq.31
16: **end if**
17: **end for**
18: **end for**
19: Step 3: Choose the most appropriate solution for the population using 10000 times D.
20: If the new best solution surpasses the prior best solution, the latter is used instead.
21: Step 4: If the end-point criteria have not been met, travel to step 2.
22: Step 5. Report the most effective solution.
23: **end for**

Fig. 9 TSA Flow-Chart [59]

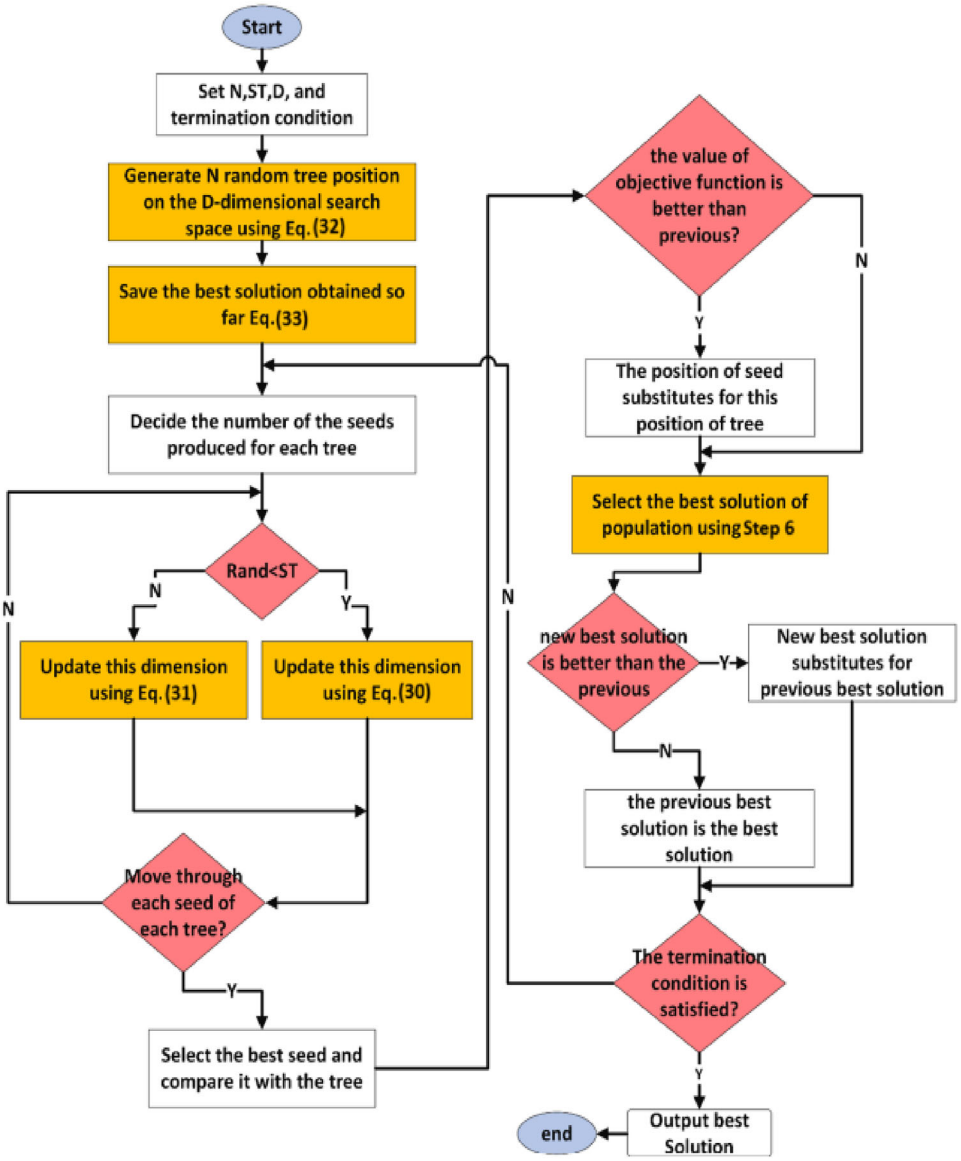

mization. Various time-domain metrics, such as over_shoot (OS), unde_ shoot (US), and settling_time (ST), are recorded and reported for all three area frequency errors and tie-bar power errors for all regulating techniques.

6.1 PS with zero communication delay

First, all four controllers are used to replicate the previously specified system without taking communication latency into account. The values for all PS settings are presented in the appendix. Table 4 lists the four distinct controller settings that have been adjusted using the suggested approach (TSA). Figures 10 and 11 combine the system's responses for the frequency error (ΔF_i) and tie-line error of power ($\Delta P_{tie_{ij}}$) for various controllers. Table 5 shows a list of time-domain details used for assessing the system performance.

Comparing the TSA:PID control to all other controlling systems, Table 5 shows that it is rated as the poorest in every category, including OS, US, and ST. TSA:IT2FLC-FOPID controller outperforms all other mentioned controllers in case of OS, US for ΔF_1, OS for ΔF_2 OS, US for ΔF_3 and US for ΔP_{tie12} with sufficiently large percentage. The effectiveness of TSA-assisted IT2FLC-(1+PD)-FOPID has been demonstrated when all other factors are held constant. The following are the suggested controller's performance evaluations: The performance is 59%, 75% better than TSA:PID for the US and 58%, 62% better than TSA:FOPID for the ST of ΔF_1. Additionally, ST is 41% better than TSA:IT2FLC-FOPID controller. In the instance of ST of ΔF_2, it performs 72%, 61%, and 44% better than TSA:PID, TSA:FOPID, and TSA:IT2FLC-FOPID. For ST of ΔF_3, it performs 72%, 54%, and 31% better than TSA:PID, TSA:FOPID, and

Table 4 Controller configurations using TSA

Area	Tuned-parameters	TSA:PID	TSA:FOPID	TSA:IT2FLC-FOPID	TSA:IT2FLC-(1+PD)-FOPID
	K_{P1}	–	–	–	4.477
	K_{D1}	–	–	–	0.729
	K_{P2}	0.452	0.547	0.274	0.136
1st	K_{I2}	0.4856	5.851	1.0625	3.642
	K_{D2}	0.9433	0.01	0.0128	0.044
	λ	–	0.01	0.0321	0.820
	μ	–	0.7741	0.3411	0.668
	K_{P1}	–	–	–	2.767
	K_{D1}	–	–	–	0.294
	K_{P2}	0.582	0.573	0.714	0.411
2nd	K_{I2}	0.462	5.571	1.285	2.472
	K_{D2}	0.833	0.361	0.218	0.474
	λ	–	0.523	0.188	0.431
	μ	–	0.271	0.317	0.58
	K_{P1}	–	–	–	2.697
	K_{D1}	–	–	–	0.229
	K_{P2}	0.251	0.740	0.444	1.941
3rd	K_{I2}	0.816	1.581	1.215	4.402
	K_{D2}	0.773	0.518	0.833	0.42
	λ	–	0.65	0.321	0.796
	μ	–	0.774	0.91	0.89

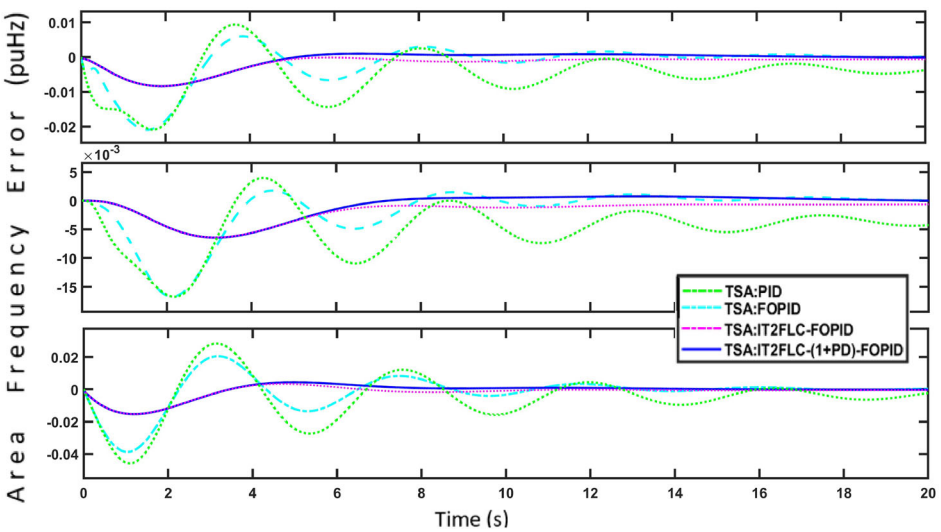

Fig. 10 Frequency variations in all sectors with no communication delay

TSA:IT2FLC-FOPID. Similar results are also observed in the case of tie-bar power failures, as Fig. 11 and Table 5 demonstrate. The recommended controller outperforms TSA:PID, TSA:FOPID, and TSA:IT2FLC-FOPID in terms of ST by about 81%, 61%, and 56%, respectively, for both ΔP_{tie12} and ΔP_{tie12}.

6.2 PS with delay in communication

The identical set of controllers, taking into account FOPTD with all three areas, simulates the same three-area hybrid, deregulated, linked electricity system. While additional optimization techniques like PSO, LMA, and FSO are also utilized to adjust the settings of the IT2FLC-(1+PD)-FOPID controller, only TSA serves to optimize the settings of the PID, FOPID, and IT2FLC-FOPID controllers. Here, the

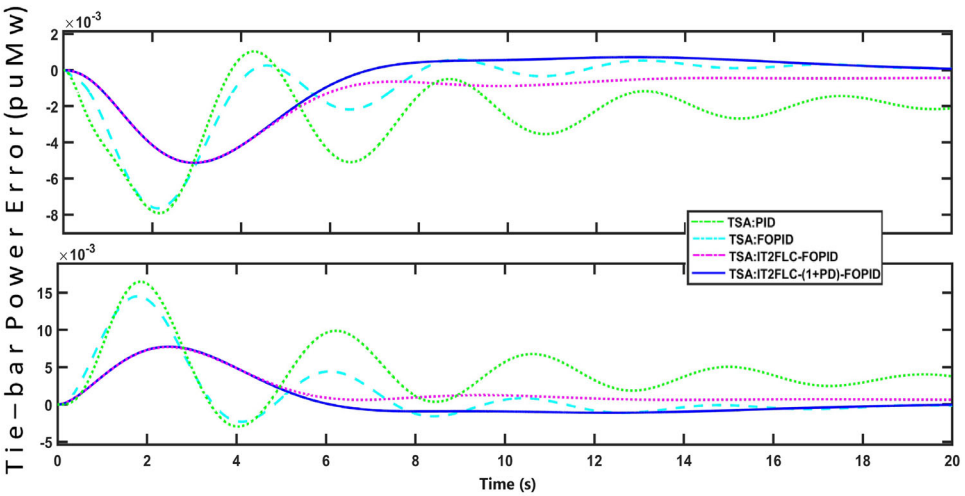

Fig. 11 Tie-line power error in all areas with zero communication delay

Table 5 Time-domain outcomes for the system with different control strategies and no communication lag

Function	Parameters	Three-area hybrid system			
		TSA:PID	TSA:FOPID	TSA:IT2FLC-FOPID	TSA:IT2FLC-(1+PD)-FOPID
	OS	0.00976	0.00662	0	0.000012
Δf_1	US	−0.0207	−0.0202	−0.0085	−0.0085
	ST	29.87	19.45	12.66	7.43
	OS	0.0048	0.0034	0	0.00008
Δf_2	US	−0.00634	−0.00624	−0.0064	−0.0064
	ST	32.03	22.52	15.81	8.82
	OS	0.0318	0.0205	0.000065	0.000068
Δf_3	US	−0.0463	−0.0394	−0.0177	−0.0177
	ST	28.35	17.45	11.66	8.03
	OS	0.0017	0.00065	0.000648	0
ΔP_{tie12}	US	−0.00792	−0.00788	−0.00522	0.00522
	ST	52.35	25.45	22.66	10.03
	OS	0.0178	0.0149	0.00765	0.00758
ΔP_{tie13}	US	−0.0031	−0.0028	−0.00177	0
	ST	54.35	27.45	26.66	11.59

authors have attempted to construct a performance comparison between several controller and optimization technique pairings for the power system based on FOPTD. In Table 6, controller configurations with various optimizations are developed. For every region, a time-varying communication delay of one to ten seconds is taken into account for each controlling strategy. The characteristics of the tie-line power errors and the frequency errors of three different system regions are depicted in Figs. 12 and 13, respectively. Table 7 tabulates the results obtained from Figs. 12 and 13.

According to the findings displayed in Figs. 12 & 13, the TSA-adjusted recommended controller (TSA:IT2FLC-(1+PD)-FOPID) performs remarkably better than TSA:PID and TSA:FOPID with 97–100% in each time-domain requirements (OS, US, and ST) of all three regions. The recommended controller outperforms TSA:IT2FLC-FOPID in all three areas, with an OS improvement of 88-100%, a frequency error improvement of 8–10%, and a tie-bar power error improvement of 38–98%. Furthermore, the recommended controller performs 2–28% better for ST than TSA:IT2FLC-FOPID. Therefore, TSA:IT2FLC-(1+PD)-FOPID is the best controller among the three used in this study for FOPTD-based renewable hybrid PS networks.

The authors then shifted the focus of their investigation to compare several optimization techniques using the same controller (IT2FLC-(1+PD)-FOPID). TSA, FSO, and LMA provide similar findings for OS for $Del F_i$, as shown in Figs. 12 & 13. The proposed algorithm (TSA) performs better than the other algorithms with 67–82% US in $Del F_1$, 65-80% US in $Del F_2$, 55-71% US in $Del F_3$, 45-47% ST

Table 6 Parameter settings of the different controller-optimization pairs for FOPTD-based power system

Area	Parameters	TSA PID	TSA FOPID	TSA IT2FLC-FOPID	PSO	FSO	LMA	TSA
					I T 2 F L C - (1 + P D) - F O P I D			
	K_{P1}	–	–	–	6.872	3.812	2.004	4.477
	K_{D1}	–	–	–	5.218	2.92	0.529	0.729
	K_{p2}	0.582	0.793	0.374	2.334	1.763	4.297	0.136
1st	K_{i2}	0.876	3.541	1.725	6.443	2.224	1.576	3.642
	K_{d2}	1.437	1.664	0.162	0.876	0.662	1.334	0.044
	λ	–	5.81	4.315	2.983	0.884	0.612	0.820
	μ	–	3.7741	1.3411	0.590	0.981	1.560	0.668
	K_{P1}	–	–	–	1.884	2.612	1.652	2.767
	K_{D1}	–	–	–	2.901	1.113	2.612	0.294
	K_{p2}	0.052	0.057	0.074	0.721	0.712	1.130	0.411
2nd	K_{i2}	0.815	3.851	2.651	2.245	1.451	4.440	2.472
	K_{d2}	0.453	0.156	0.280	1.492	1.402	0.950	0.474
	λ	–	0.603	0.216	0.32	0.76	0.501	0.431
	μ	–	0.743	0.613	0.561	0.773	0.861	0.58
	K_{P1}	–	–	–	1.117	3.339	2.491	2.697
	K_{D1}	–	–	–	0.982	0.774	1.572	0.229
	K_{p2}	5.52	2.571	0.249	1.934	2.269	0.774	1.941
3rd	K_{i2}	0.596	4.516	4.615	0.884	2.082	1.003	4.402
	K_{d2}	1.423	1.13	0.298	2.569	4.523	2.226	0.42
	λ	–	0.91	0.61	0.726	0.723	0.664	0.796
	μ	–	0.715	0.371	0.981	0.772	0.378	0.89

in $Del\,F_1$, 41-44% ST in $Del\,F_2$, and 44-51% ST in $Del\,F_3$, respectively. In the case of $Del\,P_{ties}$ across different areas, the proposed method outperforms all current optimization strategies with 44-98% better OS, 17-85% better US, and 35-62% better ST. Only in the US of $Del\,P_{tie12}$ LMA and the OS of $Del\,P_{tie13}$ PSO does it outperform TSA.

The frequency response (Bode plot) of the various controller-optimization combinations is shown in Fig. 14. As the phase and gain margins are determined to be limitless, all controllers reach their stability. It suggests that the system is stable and resistant to oscillations and instability due to its significant phase margin and safety margin against gain fluctuations, guaranteeing resilience against changes in system parameters or operating circumstances. A summary of the frequency investigation of various PS components with various regulating actions is shown in Table 8.

7 Robustness analysis of IT2FLC-(1+PD)-FOPID controller

By taking into account a time-varying FOPTD to the third area, where the OTPP is integrated into the hybrid PS, a random load type of load perturbation (RLP) is accomplished to test the resilience of the IT2FLC-(1+PD)-FOPID controller using the recommended TSA algorithm. The load value of the RLP type varies by $\pm$ 20% or 0.02 p.u (Mw). The reliability of the suggested controller is compared for several algorithms. Figure 15 depicts the RLP deployed to the recommended hybrid PS, as well as resilience findings for various regulating strategies. The findings show that to oversee a reasonable load for the selected AGC, the recommended TSA-based IT2FLC-(1+PD)-FOPID with storage device achieves the optimum solution quality for time variable delays (FOPTD).

7.1 Pros and cons of the controller

The advantages of IT2FLC-(1+PD)-FOPID are as follows:

- The IT2FLC unit handles uncertainty more effectively, such as sensor noise, model imperfections, and unmodeled dynamics.
- Improved performance in dynamic environments due to the proposed controller's multi-layer capabilities.
- The controller's sensitivity to parameter variations is reduced since it uses interval type-2 fuzzy action.
- Improved steady-state performance as the middle unit contains the '1' term along with proportional and derivative functions.
- Enhanced flexibility and precision as it has a large scope of tunable parameters

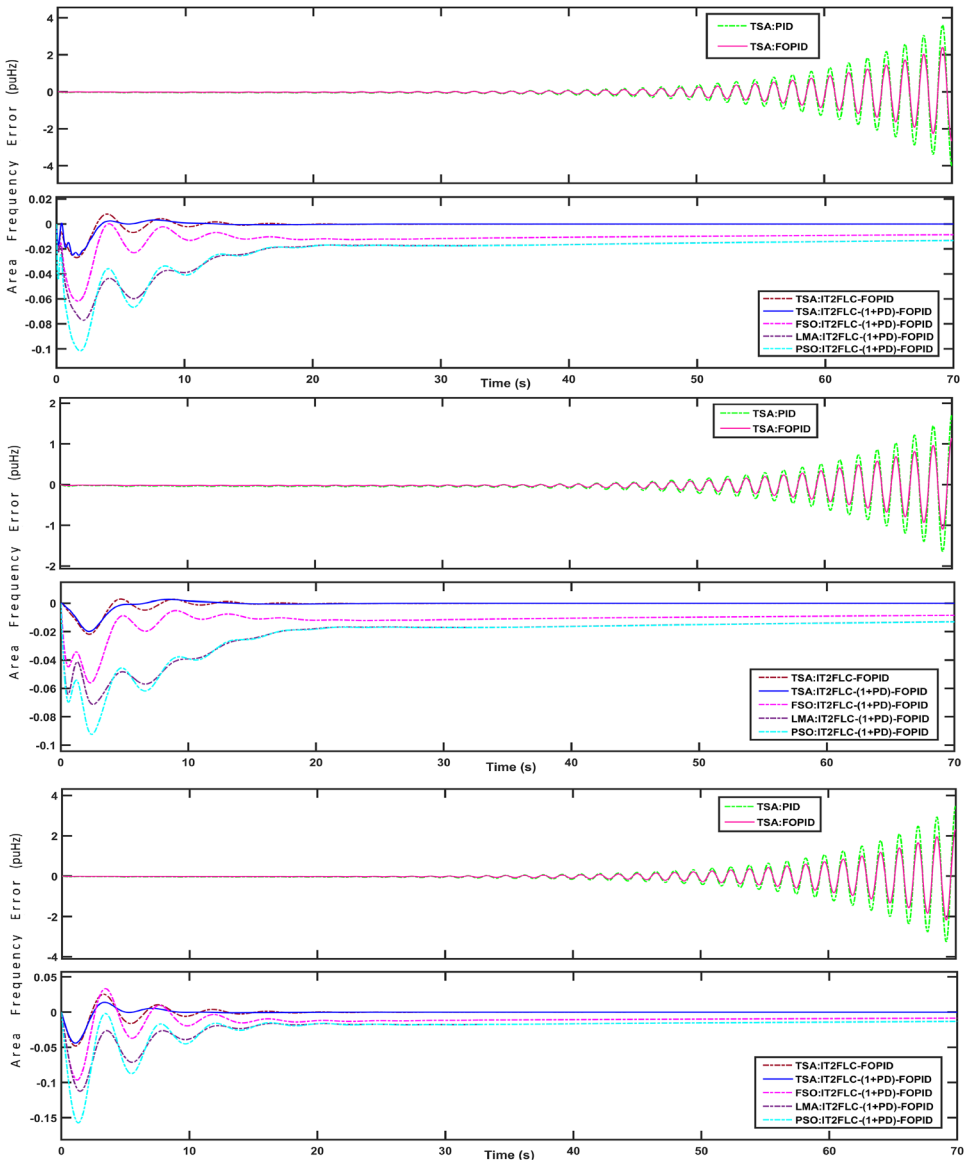

Fig. 12 Fluctuations of frequency in all three areas with delay

The disadvantages of IT2FLC-(1+PD)-FOPID are listed below:

- Increased computational complexity due to the controller's multi-layer functioning.
- Another weakness of the controller is its complexity in design and tuning.
- A longer response time is required than with basic controllers.

8 Conclusion

This article focuses on managing frequency variation in different sections of the deregulated, hybrid power system that are interconnected. It considers the AE-FC-UC storage system, different boiler limitations (such as GDB and BD), and first-order plus variable time delay. To regulate the aforementioned complicated PS, the authors proposed that TSA adjust IT2FLC-(1+PD)-FOPID in this particular case. The authors looked at four different techniques for controlling PS with TSA:PID, TSA:FOPID, TSA:IT2FLC-(1+PD), and the proposed controller, where the TSA:IT2FLC-(1+PD)-FOPID controller provides the best dynamic response of all the methods. For every power system region, a variable FOPTD (refer to Eq. 16) with a range of 0 to 10 s is taken into account for all control techniques. The results from Table 4 support the conclusion that the suggested controller provides better stability than other controllers taken into consideration in this work. Figures 10 and 11 provide the conclusion about the stable dynamic response of the same system without any kind of communication delay. When TSA-tailored IT2FLC-

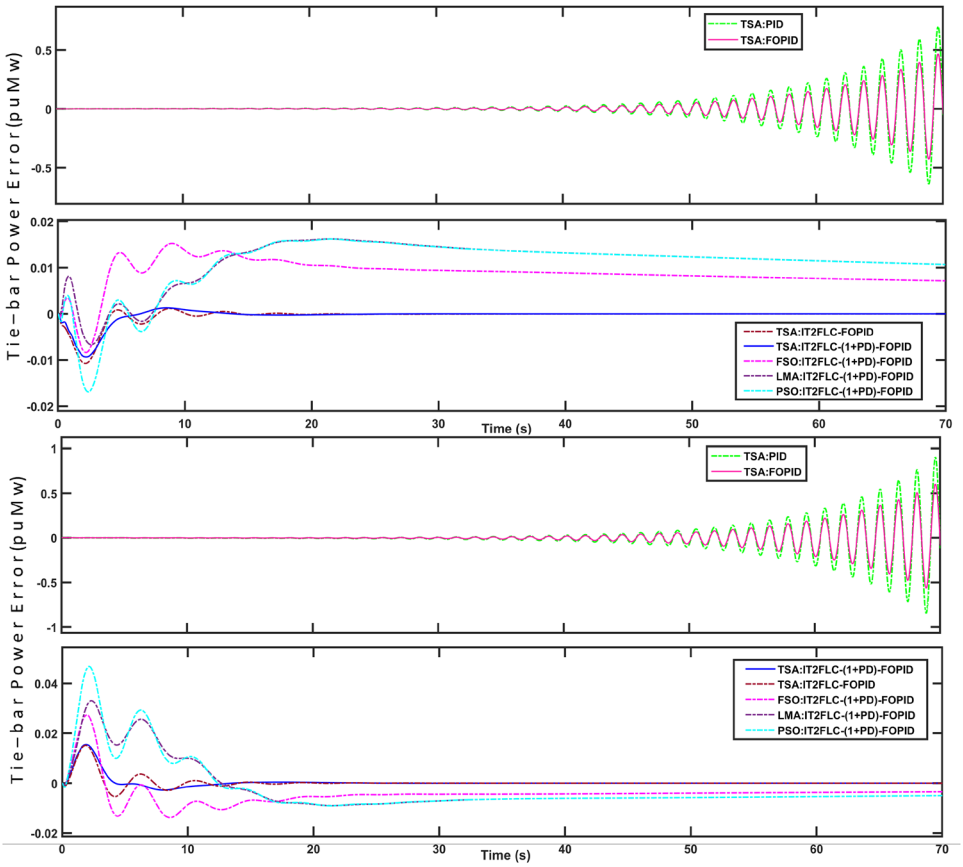

Fig. 13 Fluctuations of power in all three areas with delay

Table 7 Time-domain outcomes of the system using different control strategies with FOPTD (1-10 s)

Function	Parameters	TSA PID	TSA FOPID	TSA IT2FLC-FOPID	PSO	FSO	LMA	TSA IT2FLC-(1 + P D)-FOPID
	OS	3.98	2.11	0.084	0.000955	0	0	0
Δf_1	US	−4.05	−2.14	−0.022	−0.113	−0.0611	−0.078	−0.020
	ST	NA	NA	14.46	21.077	20.25	20.56	11.17
	OS	1.96	1.07	0.0076	0	0	0	0
Δf_2	US	−1.85	−1.03	−0.0218	−0.0968	−0.0562	−0.071	−0.0197
	ST	NA	NA	13.32	18.82	18.78	19.83	11.13
	OS	3.96	2.12	0.242	0.0013	0	0	0.016
Δf_3	US	−3.81	−2.07	−0.049	−0.153	−0.099	0.115	−0.045
	ST	NA	NA	13.46	18.07	17.95	20.23	9.98
	OS	0.768	0.482	0.0026	0.0183	0.0157	0.0092	0.0003
ΔP_{tie12}	US	−0.72	−0.46	−0.013	−0.0178	−0.00972	−0.0081	−0.0092
	ST	NA	NA	14.53	28.32	19.76	33.56	12.79
	OS	0.86	0.54	0.018	0.01574	0.028	0.034	0.018
ΔP_{tie13}	US	−0.82	−0.51	−0.0019	−0.0285	−0.014	−0.009	−0.0001
	ST	NA	NA	12.43	18.87	22.24	28.56	12.13

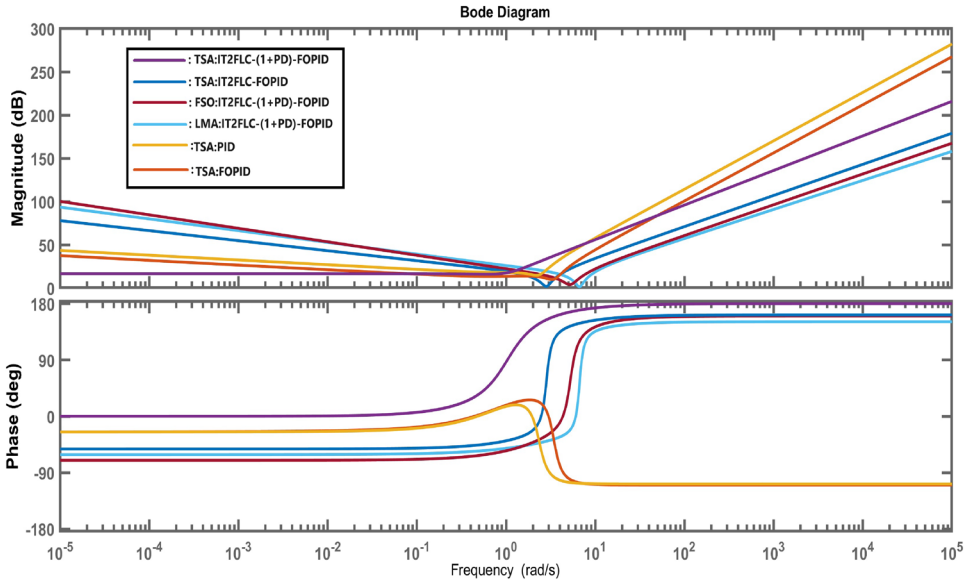

Fig. 14 Bode diagram (Magnitude plot and phase plot) for different controllers using different algorithms to illustrate the stability of the controllers

Table 8 Stability analysis utilizing phase margin (PM) and gain margin (GM) from Bode charts for time-varying FOPTD for various regions with various controllers modified by various techniques

Area	Margins	TSA PID	TSA FOPID	TSA IT2FLC-FOPID	FSO	LMA	TSA IT2FLC-(1+PD)-FOPID
1st	PM	∞	∞	∞	∞	∞	∞
	GM	∞	∞	∞	∞	∞	∞
2nd	PM	∞	∞	∞	∞	∞	∞
	GM	∞	∞	∞	∞	∞	∞
3rd	PM	∞	∞	∞	∞	∞	∞
	GM	∞	∞	∞	∞	∞	∞

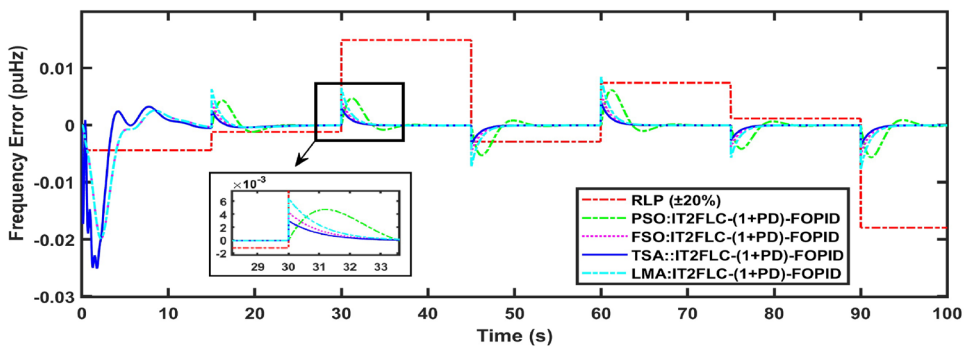

Fig. 15 Robust control scheme of IT2FLC-(1+PD)-FOPID using different algorithms with FOPTD-type communication delay

(1+PD)-FOPID is used to manage the PS with FOPTD in a later stage, the system exhibits a stable dynamic response, as shown in Figs. 12 and 13. Table 7 presents the time-domain results. It is evident that the optimal control is provided by IT2FLC-(1+PD)-FOPID when the controller parameters are tuned using the TSA method. The tight loop stability while using the PS illustrated in Fig. 1 is also determined by the controller frequency analysis, and the supporting GM & PM are tabulated in Table 8. Furthermore, it has been proved that the proposed controller is resistive to RLP of ±20%, as illustrated in Fig. 15. The authors ultimately conclude that the most suitable alternative for managing the deregulated, non-conventional energy-oriented multi-area hybrid PS load frequency issue with delay in communication is the suggested TSA-tuned IT2FLC-(1+PD)-FOPID controller. In the future, the technique provided here might be expanded to incorporate the following research projects:

- Using FOPTD for load frequency management in multiple area PS with four or more areas.

- Use an advanced multilayer control scheme, such as machine learning, sliding mode, and model predictive, to regulate the dynamic time-delayed response.
- A number of techniques, including empirical Bode analysis, may be utilized to assess the permissible range of the delay for this recommended controller in an environment of random delay in multi-area systems (MAS).

Appendix

A = 0.06; B = 0.75; F = 0.2; G = 1.0; $K_r = 0.3s$; $T_r = 10s$; $T_t = 1.25s$; $K_{SG} = 1$; $T_{SG} = 0.08$s;$T_t = 1.25s$;; K_G= 0.5; K_T = 1;$T_G = 0.08s$; $T_T = 0.3s$; K_B = 1; K_{t1} = 1; K_g = 0.5; T_{t1}= 1.25s; T_{g1}= 0.5s; $K_{GH} = T_{GH}$= 85; K_{RS} = 5; T_{RS} = 0.513s; T_W = 1; K_{Psi}= 120; T_{Psi}= 20;T_{ij} = 0.3s;$\beta_i = 0.425p.u$; $R_i = 2.4Hz/pu$ K_2 = 0.5;K_3 = 0.5;K_{IB} = 0.65;T_{IB} = 0.5s;T_{RB} = 1.2s; $\tau = 7.365s$;T_D = 0.75s;C_B = 225; T = 8 s; $G_{ff} = 0.5$ $RLP = \pm 0.02p.u(Mw)$. $A_{11} = 0.35$;$A_{12} = 0.50$;$A_{13} = 0.15$; $A_{14} = 0.2$; $A_{21} = 0.15$; $A_{22} = 0.25$;$A_{23} = 0.25$; $A_{24} = 0.1$;$A_{31} = 0.3$;$A_{32} = 0.15$; $A_{33} = 0.3$; $A_{34} = 0.4$; $A_{41} = 0.3$;$A_{42} = 0.4$; $A_{43} = 0.3$;$A_{44} = 0.3$

References

1. Arya Y (2023) ICA assisted FTIλDN controller for AGC performance enrichment of interconnected reheat thermal power systems. J Ambient Intell Humaniz Comput 14(3):1919–1935
2. Biswas S, Roy PK, Chatterjee K (2023) Development of MADB of P-I controller using LMI technique in a renewable energy based AGC system and study its application in a deregulated environment including energy storage device. Optimal Control Appl Methods 44(2):426–451
3. Bevrani H, Golpîra H, Messina AR, Hatziargyriou N, Milano F, Ise T (2021) Power system frequency control: an updated review of current solutions and new challenges. Electr Power Syst Res 194:107114
4. Doan DV, Nguyen K, Thai QV (2022) Load-frequency control of three-area interconnected power systems with renewable energy sources using novel PSO∼ PID-like fuzzy logic controllers. Eng Technol Appl Sci Res 12(3):8597–8604
5. Hu H, Yu SS, Trinh H (2024) A review of uncertainties in power systems-modeling, impact, and mitigation. Designs 8(1):10
6. Muyizere D, Letting LK, Munyazikwiye BB (2022) Effects of communication signal delay on the power grid: a review. Electronics 11(6):874
7. Ghany A eHA, Ahmed ES, ELGebaly AE (2021) A reliable loss of excitation protection technique based on EPFA for synchronous generators. IEEE Trans Power Deliv 37(3):1445–1455
8. Chakraborty S, Mondal A, Biswas S, Roy PK (2023) Design of FUZZY-3DOF-PID controller for an ocean thermal hybrid automatic generation control system. Sci Iran. https://doi.org/10.24200/sci.2023.62325.7774
9. Chakraborty S, Mondal A, Biswas S (2023) Design of type-2 fuzzy controller for hybrid multi-area power system. Fuzzy Logic Appl Comput Sci Math 78:107–124
10. Babu NR, Bhagat SK, Saikia LC, Chiranjeevi T (2020) Application of hybrid crow-search with particle swarm optimization algorithm in AGC studies of multi-area systems. J Discret Math Sci Cryptogr 23(2):429–439
11. Yeboah SJ et al (2021) Gravitational search algorithm based automatic load frequency control for multi-area interconnected power system. Turk J Comput Math Educ (TURCOMAT) 12:4548–4568
12. Liu Z, Liu W, Wang P et al (2023) High-precision position tracking control of giant magnetostrictive actuators using fractional-order sliding mode control with inverse Prandtl-Ishlinskii compensator. Int J Precis Eng Manuf 24(3):379–393
13. Nosheen T, Ali A, Chaudhry MU et al (2023) A fractional order controller for sensorless speed control of an induction motor. Energies 16(4):1901
14. Yavuz M, Özköse F, Susam M, Kalidass M (2023) A new modeling of fractional-order and sensitivity analysis for hepatitis-b disease with real data. Fractal Fract 7(2):165
15. Ngo HT, Razzaghi M, Vo TN (2023) Fractional-order Chelyshkov wavelet method for solving variable-order fractional differential equations and an application in variable-order fractional relaxation system. Numer Algorithms 92(3):1571–1588
16. Naderipour A, Abdul-Malek Z, Davoodkhani IF, Kamyab H, Ali RR (2023) Load-frequency control in an islanded microgrid PV/WT/FC/ESS using an optimal self-tuning fractional-order fuzzy controller. Environ Sci Pollut Res 30(28):71677–71688
17. Shouran M, Anayi F, Packianather M, Habil M (2022) Different fuzzy control configurations tuned by the bees algorithm for LFC of two-area power system. Energies 15(2):657
18. Hakimuddin N, Khosla A, Garg JK (2022) Comparative performance investigation of genetic algorithms (GAs), particle swarm optimization (PSO) and bacteria foraging algorithm (BFA) based automatic generation control (AGC) with multi source power plants (MSPPs). Electr Power Compon Syst 49(20):1513–1524
19. Arandian B, Eslami M, Khalid SA et al (2022) An effective optimization algorithm for parameters identification of photovoltaic models. IEEE Access 10:34069–34084
20. Eslami M, Babaei B, Shareef H, Khajehzadeh M, Arandian B (2021) Optimum design of damping controllers using modified sperm swarm optimization. IEEE Access 9:145592–145604
21. Toolabi Moghadam A, Aghahadi M, Eslami M, Rashidi S, Arandian B, Nikolovski S (2022) Adaptive rat swarm optimization for optimum tuning of SVC and PSS in a power system. Int Trans Electr Energy Syst 2022(1):4798029
22. Mohanty B (2019) Performance analysis of moth flame optimization algorithm for AGC system. Int J Model Simula 39(2):73–87
23. Goswami L, Biswas S, Dutta S, Roy PK (2017) Load frequency control of multi area power system with de-regulation using okha. In: IEEE. 507–512
24. Elsisi M, Bazmohammadi N, Guerrero JM, Ebrahim MA (2021) Energy management of controllable loads in multi-area power systems with wind power penetration based on new supervisor fuzzy nonlinear sliding mode control. Energy 221:119867
25. Nayak JR, Shaw B, Sahu BK (2020) Hybrid alopex based DECRPSO algorithm optimized Fuzzy-PID controller for AGC. J Eng Res 8:1
26. Biswas S, Roy PK, Chatterjee K (2023) FACTS-based 3DOF-PID controller for LFC of renewable power system under deregulation using GOA. IETE J Res 69(3):1486–1499
27. Hashim FA, Houssein EH, Hussain K, Mabrouk MS, Al-Atabany W (2022) Honey badger algorithm: new metaheuristic algorithm for solving optimization problems. Math Comput Simul 192:84–110
28. Sahu J, Satapathy P, Mohanty PK, Sahu BK, Nayak JR, Naik A (2024) Optimally designed fuzzy-based controller using Craziness-based CSA technique for AGC performance enhancement of power system. Electr Eng 106(1):1053–1077
29. Chen G, Qin F, Long H, Zeng X, Kang P, Zhang J (2022) Fuzzy PID controller optimized by improved gravitational search algorithm for load frequency control in multi-area power system. IAENG Int J Comput Sci 49(1):125–139

30. Mohapatra AK, Mohapatra S, Sahu PC, Debdas S (2024) Modeling of flexible AC transmission system devices and fuzzy controller for automatic generation control of electric vehicle-injected power system. e-Prime-Adv Electr Eng Electron Energy 7:100483
31. Sahu PC (2024) Impact and integration of electric vehicles on renewable energy based microgrid: frequency profile improvement by a-SCA optimized FO-Fuzzy PSS approach. Green Energy Intell Transp 4:100191
32. Sahu PC, Samantaray SR (2023) Resilient frequency stability of a PV/wind penetrated complex power system with CSA tuned robust Type-2 fuzzy cascade PIF controller. Electr Power Syst Res 225:109815
33. Aryan P, Raja GL (2022) Analysis of Type-2 Fuzzy I λ D μ-P Controller for LFC with Communication Delay. In: IEEE. ; 01–07
34. Chakraborty S, Mondal A, Biswas S (2024) Application of FUZZY-3DOF-PID controller for controlling FOPTD type communication delay based renewable three-area deregulated hybrid power system. Evolut Intell 17:1–21
35. De AK, Chakraborty D, Biswas A (2022) Literature review on type-2 fuzzy set theory. Soft Comput 26(18):9049–9068
36. Bhatta SK, Mohapatra S, Sahu PC, Swain SC, Panda S (2023) Novel QO-PFA governed FO-type-II fuzzy controller for LFC of thermo-electric generator based hybrid power system. e-Prime-Adv Electr Eng Electron Energy 5:100249
37. Arya Y, Kumar N, Dahiya P et al (2021) Cascade-IλDμN controller design for AGC of thermal and hydro-thermal power systems integrated with renewable energy sources. IET Renew Power Gener 15(3):504–520
38. Kiran MS, Yunusova P (2022) Tree-seed programming for modelling of Turkey electricity energy demand. Int J Intell Syst Appl Eng 10(1):142–152
39. Karthik E, Sethukarasi T (2022) Sarcastic user behavior classification and prediction from social media data using firebug swarm optimization-based long short-term memory. J Supercomput 78:1–25
40. Esfe MH, Toghraie D, Amoozadkhalili F (2023) Optimization and design of ANN with Levenberg-Marquardt algorithm to increase the accuracy in predicting the viscosity of SAE40 oil-based hybrid nano-lubricant. Powder Technol 415:118097
41. Gharehchopogh FS (2022) Advances in tree seed algorithm: a comprehensive survey. Arch Comput Method Eng 29(5):3281–3304
42. Biswas S, Mahata S, Roy PK, Chatterjee K (2023) Application of empirical bode analysis for delay-margin evaluation of fractional-Oorder PI controller in a renewable distributed hybrid system. Fractal Fract 7(2):119
43. Ashjaee M, Tavazoei M (2022) Tuning the implementable structures of fractional-order PID controllers for control of FOPDT processes. Sci Iran 29(2):660–675
44. Podlubny I (1999) Fractional-order systems and PIλDμ-controllers. IEEE Trans Autom Control 44:208–214
45. Ansarian A, Mahmoodabadi M (2023) Multi-objective optimal design of a fuzzy adaptive robust fractional-order PID controller for a nonlinear unmanned flying system. Aerosp Sci Technol 141:108541
46. Dash PM, Baliarsingh AK, Mohapatra SK (2023) Hybrid African vulture optimization algorithm and pattern search tuned fractional order PID controller for AGC of electric vehicles integrated power systems. Int J Electr Eng Inform 15(2):259–276
47. Karanam AN, Shaw B, Nayak JR (2022) Implementation of Crow Search Algorithm based two degree of freedom combined fractional order PID controller for AGC of hydro-thermal power system with wind and small hydro power plants
48. Mondal A, Chakraborty S (2024) Design of two-loop FOPID-FOPI controller for inverted cart-pendulum system. Eng Res Express 6(3):035354
49. Çelik E, Öztürk N, Arya Y, Ocak C (2021) (1+ PD)-PID cascade controller design for performance betterment of load frequency control in diverse electric power systems. Neural Comput Appl 33(22):15433–15456
50. Shafei MAR, Ibrahim DK, Bahaa M (2022) Application of PSO tuned fuzzy logic controller for LFC of two-area power system with redox flow battery and PV solar park. Ain Shams Eng J 13(5):101710
51. Soliman AMA, Bahaa M, Mehanna MA (2023) PSO tuned interval type-2 fuzzy logic for load frequency control of two-area multi-source interconnected power system. Sci Rep 13(1):8724
52. Zadeh LA (1975) The concept of a linguistic variable and its application to approximate reasoning-I. Inf Sci 8(3):199–249
53. Reyes-García CA, Torres-Garcia AA (2022) Fuzzy logic and fuzzy systems. In: Elsevier. (pp. 153–176)
54. Zhao T, Chen C, Cao H, Dian S, Xie X (2022) Multiobjective optimization design of interpretable evolutionary fuzzy systems with type self-organizing learning of fuzzy sets. IEEE Trans Fuzzy Syst 31:1638
55. Srivastava V, Sharma U, Schaub J, Pischinger S (2024) Adaptive control concepts using radial basis functions and a Kalman filter for embedded control applications. Int J Eng Res 25(1):125–139
56. Mendel JM (2017) Uncertain rule-based fuzzy systems. Introduction and new directions 684
57. Hwang C, Cheng YC (2021) On calculation of ISE performance indices for fractional-order time-delay systems. J Taiwan Inst Chem Eng 120:17–23
58. Aguilera-Verdugo JJ, Hernández-Pinto RJ, Rodrigo G, Sborlini GF, Torres Bobadilla WJ (2021) Mathematical properties of nested residues and their application to multi-loop scattering amplitudes. J High Energy Phys 2021(2):1–42
59. Köse E (2020) Optimal control of AVR system with tree seed algorithm-based PID controller. IEEE Access 8:89457–89467